ELSEVIER

Nuclear Instruments and Methods in Physics Research A 490 (2002) 146–158

NUCLEAR INSTRUMENTS & METHODS IN PHYSICS RESEARCH Section A

www.elsevier.com/locate/nima

The AGILE silicon tracker: testbeam results of the prototype silicon detector

G. Barbiellini[a], G. Fedel[a], F. Liello[a], F. Longo[b], C. Pontoni[c], M. Prest[c,*], M. Tavani[d], E. Vallazza[e]

[a] *Università degli Studi di Trieste and INFN, sezione di Trieste, Italy*
[b] *Università degli Studi di Ferrara and INFN, sezione di Ferrara, Italy*
[c] *CIFS - Consorzio Interuniversitario per la Fisica Spaziale and INFN, sezione di Trieste, Padriciano 99, 34012 Trieste, Italy*
[d] *Istituto di Fisica Cosmica, CNR, Milano, Italy*
[e] *INFN, sezione di Trieste, Italy*

Received 2 May 2001; received in revised form 7 November 2001; accepted 3 March 2002

Abstract

AGILE (Light Imager for Gamma-ray Astrophysics) is a small scientific satellite for the detection of cosmic γ-ray sources in the energy range 30 MeV–50 GeV with a very large field of view (1/4 of the sky). It is planned to be operational in the years 2003–2006, a period in which no other γ-ray mission in the same energy range is foreseen.

The heart of the AGILE scientific instrument is a silicon–tungsten tracker made of 14 planes of single sided silicon detectors for a total of 43 000 readout channels. Each detector has a dimension of $9.5 \times 9.5\ cm^2$ and a thickness of 410 μm.

We present here a detailed description of the performance of the detector prototype during a testbeam period at the CERN PS in May 2000. The Tracker performance is described in terms of position resolution and signal-to-noise ratio for on and off-axis incident charged particles. The measured 40 μm resolution for a large range of incident angles will provide an excellent angular resolution for cosmic γ-ray imaging.

PACS: 07.50.Qx; 29.30.Kv; 29.40.Wk; 95.55Ka

Keywords: Satellite; Silicon detector; Self triggering; Floating strip; γ-ray detector

1. Introduction

The Astrorivelatore Gamma a Immagini LEggero—Light Imager for γ-ray Astrophysics (AGILE) mission has been approved by the Italian Space Agency (ASI) in 1998 and has just entered the construction phase. AGILE will provide a powerful observatory for γ-ray astrophysics in the energy range 30 MeV–50 GeV, during the years 2003–2006. No other γ-ray mission in this energy range is planned in the same period.

The instrument is light (≈100 kg) and effective in detecting and monitoring γ-ray sources within a large field of view (≈1/4 of the whole sky). The instrument consists of a silicon–tungsten Tracker, a $1.5X_0$ deep CsI(Tl) minicalorimeter,

*Corresponding author. Tel.: +39-040-3756253; fax: +39-040-3756258.

E-mail address: michela.prest@ts.infn.it (M. Prest).

0168-9002/02/$ - see front matter
PII: S0168-9002(02)01062-8

an anticoincidence system made of segmented plastic scintillators, a X-ray detector in the range 10–40 keV with a coded mask system, fast readout electronics and processing units.

The working principle of AGILE is shown in Fig. 1: the photon converts in an electron–positron pair in the Tracker tungsten layers and is detected by the silicon strips. The CsI(Tl) minicalorimeter measures the energy released by the electron and the positron while the anticoincidence AC is used to reject charged particle background.

The overall dimension of the instrument is $63 \times 63 \times 58\ \mathrm{cm}^3$.

The Silicon Tracker is the heart of the AGILE mission and its design and construction are under the responsibility of INFN. It has a twofold purpose:

- to provide the trigger to the whole instrument when a γ-ray has converted inside the Tracker itself,
- to provide a complete representation of the event topology, allowing the reconstruction of the momentum and direction of the electron–positron pair produced by the photon conversion and thus the incoming direction of the γ-ray itself.

In the following, we present the features of the AGILE silicon detector (Section 2) and the testbeam results we have obtained with the final silicon prototypes (Section 3).

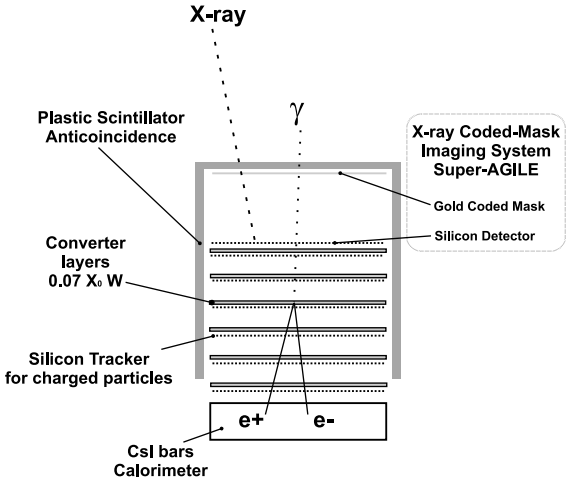

Fig. 1. Working principle of the AGILE instrument.

2. The AGILE silicon detector

The AGILE silicon detectors are single-side AC-coupled strip detectors, built on high resistivity ($\geqslant 4\ \mathrm{k}\Omega$ cm) 6″ substrate by HAMAMATSU PK. Their size is $9.5 \times 9.5\ \mathrm{cm}^2$ while their thickness is 410 μm. The biasing of the detector is achieved through polysilicon resistors.

The detector is used with a "floating strip" configuration [1]; the physical strip pitch is 121 μm and the readout one is 242 μm.

This configuration has been chosen in order to have an excellent spatial resolution while keeping under control the number of readout channels and hence the detector power consumption.

The prototype production consists of 10 detectors with the following electrical characteristics:

- Bias resistor: 40 MΩ
- Coupling capacitance (measured at 10 kHz): 527 pF
- AC coupling Al resistance: 4.5 Ω/cm
- Leakage current density at a biasing voltage 20% higher than the depletion one ($V_{\mathrm{FD}} =$ 75 V): $1.5\ \mathrm{nA/cm}^2$.

The AGILE Tracker is made of 14 planes, each organized in 2 views with 16 tiles. The strip orientation of the first view is perpendicular to the one of the second view resulting in a x–y detector.

Four silicon detectors are bonded together to create a "ladder". Each view is thus made of four ladders 38 cm long with 384 strips each.

Fig. 2 shows one of the AGILE silicon detectors, while Fig. 3 is a picture of the ladder built for the AGILE May 2000 testbeam at the CERN PS area.

3. The silicon detector performance

The final prototype of the silicon detector has been tested with the TA1 version of the frontend ASIC [3] during a testbeam period at the T11 beamline at the CERN PS (East Hall, May 1–11, 2000).

The main features of the beam are summarized in Table 1; for a detailed description, see Ref. [4].

As far as the beam particle composition is concerned, the relative fraction of the different types is shown in Fig. 4.

The main goal of the test was to study the detector behaviour before starting the final production. In the following subsections, we describe the testbeam and the detector setup and the main results we have obtained.

3.1. Testbeam setup

Fig. 5 shows the testbeam setup, which consists of:

- A Cherenkov counter for particle identification, which is part of the T11 beam instrumentation, followed by the last magnet of the T11 beamline;
- A system of two plastic scintillators (S1 and S2) of 3×5 cm^2 and 1 cm thick, for the trigger;

Table 1
Main features of the T11 beam (h = horizontal, v = vertical)

Maximum design momentum	3.5 GeV/c
Theoretical momentum resolution	1.9%
Calculated beam cross-section	18(h) × 10(v) mm^2
Production angle	149.2 mrad
Angular acceptance	±6.2(h), ±19.2(v) mrad

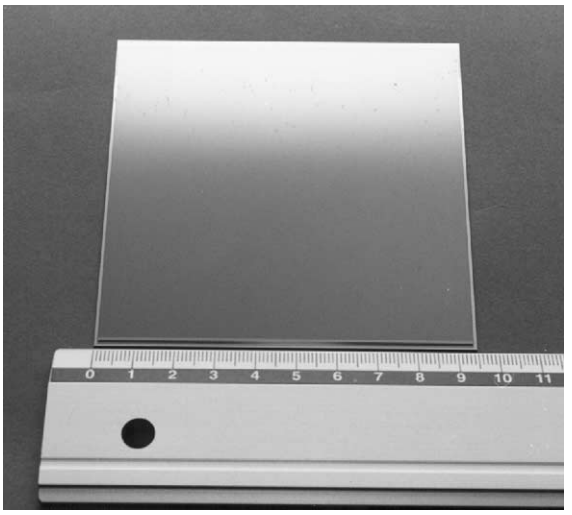

Fig. 2. The HAMAMATSU final prototype for the AGILE silicon detector.

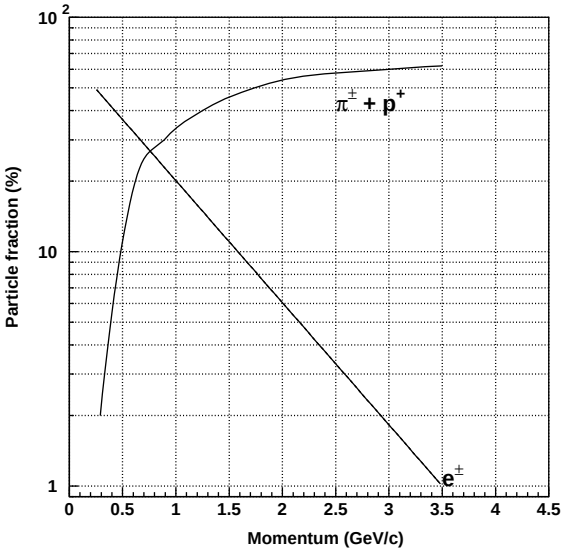

Fig. 4. Particle composition of the T11 beam as a function of the energy.

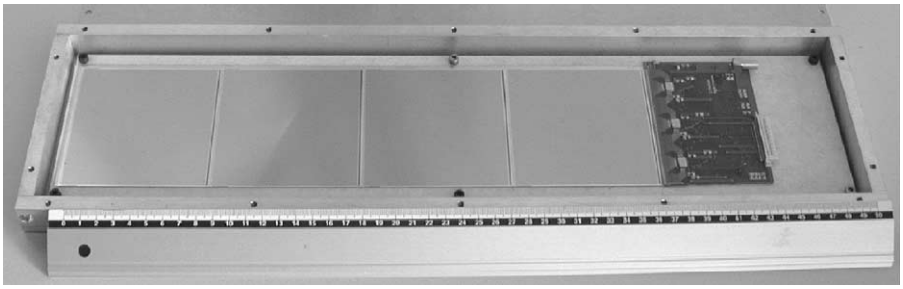

Fig. 3. Prototype ladder tested during the May 2000 testbeam at the CERN PS area; the ladder has been assembled by Mipot [2].

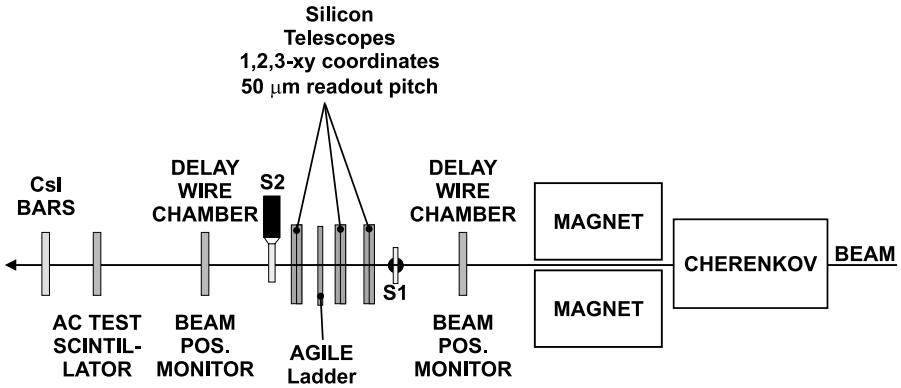

Fig. 5. Testbeam setup on the T11 beamline at the CERN PS for the May AGILE run.

- A couple of delay wire chambers [5] for the beam characterization and monitoring;
- A system of 3 x–y silicon telescopes [6] for the tracking. Each telescope is made of two single-side AC-coupled silicon detectors of $3.2 \times 3.2\ \mathrm{cm}^2$ with a readout pitch of 50 μm and a floating strip configuration; the detector read-out is based on VA2 ASICs [7];
- The detector under test (Fig. 3); it is an AGILE ladder made of four HAMAMTSU prototypes connected together with 17 μm wire bondings and readout by TA1s;
- The AGILE top anticoincidence scintillator and two of the bars of the CsI (Tl) minicalorimeter.

Fig. 6 shows the testbeam data acquisition system, which can be divided into three blocks:

- *Trigger logic*: The signals from the scintillators and the Cherenkov counter are discriminated and sent to the trigger logic for the generation of the DAQ trigger needed by the main acquisition board, the Viking Sequencer;[1] the same logic treats the TA1 trigger signals;
- *Beam monitoring*: The signals from the DWCs and the Cherenkov counter are readout by a set of TDCs (LeCroy 1176 and 2228 A) and used in the offline analysis;
- *Detector test*: The silicon strip signals (the 1280 strips of each of the three telescopes and the 384 ladder strips) are read by four 10 bit VME ADCs (Sirocco[6]) while the information of the CsI bars is read by a 10 bit ADC CAEN V550.

The anticoincidence had an independent data acquisition system which is not shown in Fig. 6.

As far as the hardware is concerned, we adopted the VME standard while the CAMAC is accessed by means of a CES CBD8210 branch driver.

The DAQ system has to fulfil the following tasks:

- Generate the timing sequence for the readout when a trigger signal is present;
- Get the information from the detectors (the DWCs, the telescopes, the ladder and the CsI bars) and write it on disk;
- Check the run conditions and the working parameters of the TA1s;
- Display the monitor histograms.

The DAQ system has been developed so that each task is controlled by a separate process. The inter-process communication is performed via TCP/IP using the RPC protocol [8].

In the present setup, all the processes run on a PC with an Athlon 500 MHz processor with the Linux operating system. The access to the VME is done through a Bit3 Mod. 617 controller [9].

The data acquisition frame relies on the Tcl/Tk package [10], which provides a flexible structure to

[1] LEPSI, Strasbourg, France.

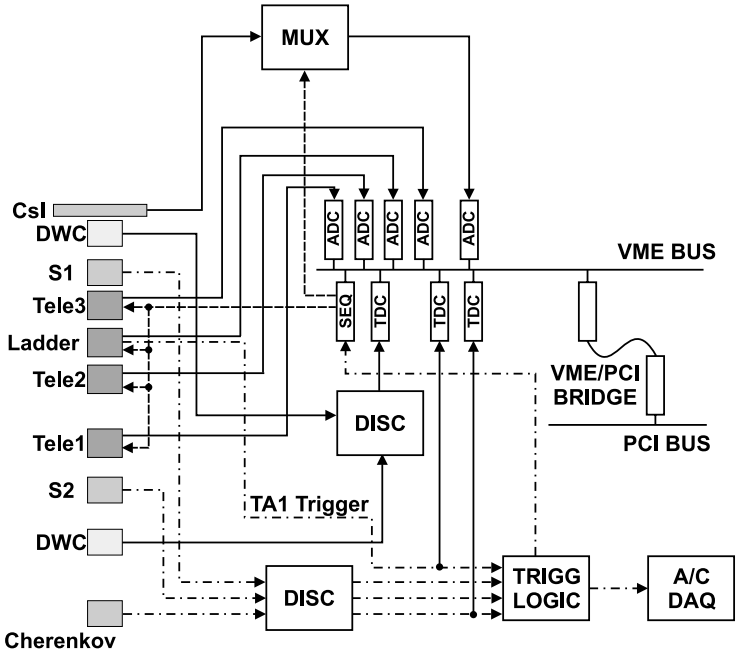

Fig. 6. Testbeam data acquisition system.

implement the different functions and to control them via a GUI.

The DAQ code is written in C and C++ while the histogramming part is built using HPLOT [11].

3.2. Testbeam results

More than 2.3 million events have been collected in order to study:

- The ladder behaviour according to the region hit by the beam (different silicon tile or different region inside the tile);
- The ladder behaviour as a function of the angle of incidence of the beam with respect to the silicon strips, in terms of cluster pulse height, signal-to-noise ratio (SNR), number of strips per cluster. The incidence angle is the angle between the beam and the plane of the silicon strip tile. The range between 30° and 90° (that is the interesting region for AGILE) has been scanned in steps of 15°. Fig. 7 defines the incidence angle of the beam: the tracks have been chosen using the y telescope information in order to guarantee that the beam is contained in a horizontal plane and the x information to select tracks with the same angle.
- The trigger efficiency of the ladder as a function of the incidence angle of the beam.

Pedestal data for all the strips are collected in dedicated runs and then analyzed offline to compute the pedestal value for each strip (mean value of the distribution of all the events) and the noise rms before and after the subtraction of the common mode.

All the results presented in the following sections have been obtained with a positive charged particle beam (mostly pions) characterized by a momentum of 2 GeV/c.

3.2.1. Noise

Given the characteristics of the detectors under test, it is possible to compute the expected noise for the AGILE ladder.

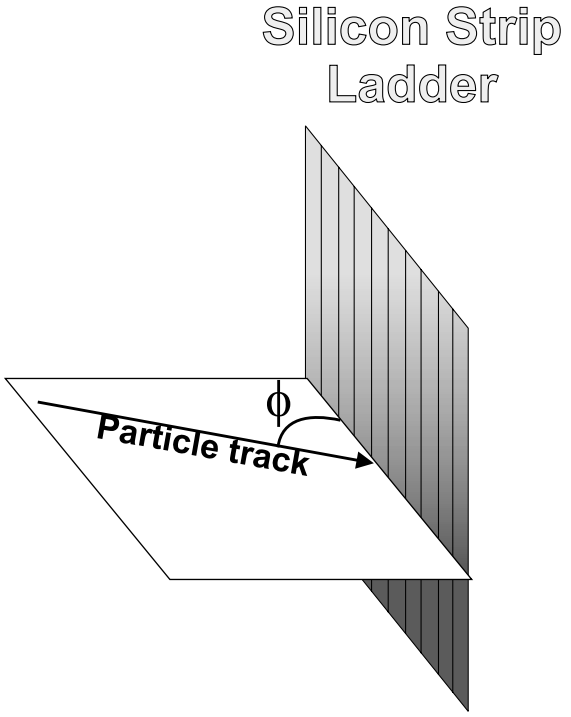

Fig. 7. Definition of the incidence angle of the beam with respect to the detector plane.

From Ref. [12], the different noise contributions are

- *From the leakage current*

$$\mathrm{ENC}_{\mathrm{leak}} = \frac{e}{q}\sqrt{qI_{\mathrm{leak}}T_{\mathrm{p}}/4}$$

where e is the natural logarithm base, q the electron charge, I_{leak} the total strip leakage current and T_{p} the shaper peaking time (in our case 5 μs);

- *From the polarization resistors*

$$\mathrm{ENC}_{\mathrm{res}} = \frac{e}{q}\sqrt{\frac{kT\,T_{\mathrm{p}}}{2R_{\mathrm{p}}}}$$

where $kT = 0.025$ eV at $T = 300$ K and R_{p} the biasing resistor;

- *From the resistance of the metal strip*

$$\mathrm{ENC}_{\mathrm{ms}} = \frac{C_{\mathrm{t}}e}{q}\sqrt{\frac{kT\,R_{\mathrm{ms}}}{6T_{\mathrm{p}}}}$$

where R_{ms} is the total resistance of the metal strip end to end and C_{t} the total strip capacitance;

- *From the readout ASIC*

$$\mathrm{ENC}_{TA1} = 165 + 6.1C_{\mathrm{t}}$$

as given by IDE AS.

The total noise is the sum in quadrature of the different components:

$$\mathrm{ENC}_{\mathrm{tot}} = \mathrm{ENC}_{TA1} \oplus \mathrm{ENC}_{\mathrm{ms}} \oplus \mathrm{ENC}_{\mathrm{res}} \oplus \mathrm{ENC}_{\mathrm{leak}}.$$

The different noise contributions expressed in rms electrons for an AGILE Silicon Tracker ladder are shown in Table 2.

The distribution of the rms noise of all the ladder channels before (13 ADC) and after the common mode (CM) subtraction (5.9 ADC) is shown in Fig. 8. The common mode component is given by the fluctuation of all the channels at the same time and is mainly due to pickup on the detector bias voltage. A too high CM could prevent the possibility of setting the trigger threshold at 1/4 of a MIP thus reducing the satellite trigger efficiency.

The CM component is computed offline for each event as

$$CM = \frac{\sum_{i=1}^{N}(\mathrm{raw}_i - \mathrm{ped}_i)}{N}$$

where raw_i is the raw content of the readout channel in ADC counts, ped_i the channel pedestal as computed using the pedestal run and N the number of "good" strips of the detector; noisy and/or dead strips are discarded.

Table 2
AGILE Silicon Tracker noise contributions for a ladder expressed in rms electrons

Noise contribution	Value (rms e-)
$\mathrm{ENC}_{\mathrm{leak}}$	227
$\mathrm{ENC}_{\mathrm{res}}$	508
$\mathrm{ENC}_{\mathrm{ms}}$	45.5
$\mathrm{ENC}_{\mathrm{TA1}}$	490
$\mathrm{ENC}_{\mathrm{tot}}$	743

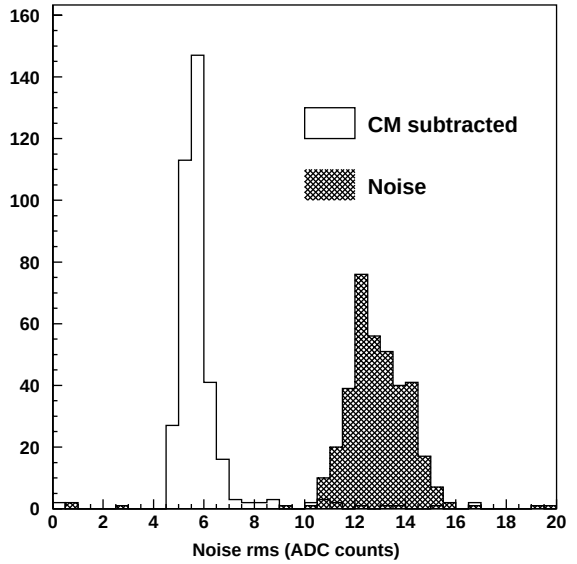

Fig. 8. Ladder noise rms before and after the CM subtraction.

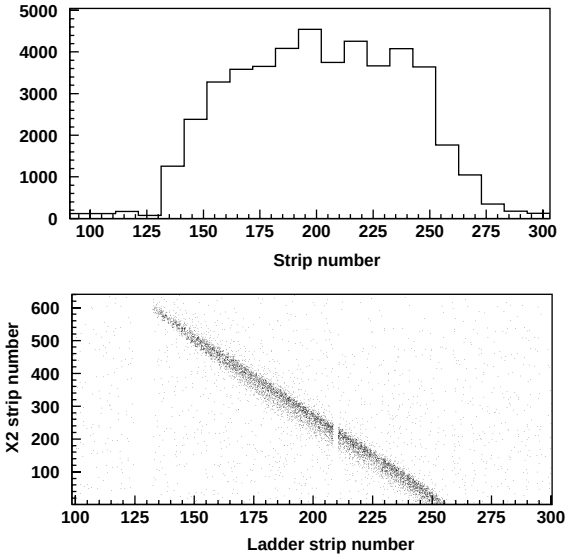

Fig. 9. Ladder beam profile (upper plot) and correlation between the ladder and one of the x telescope position (lower plot); two of the ladder strips have been excluded in the offline analysis because of their high noise.

3.2.2. Ladder behaviour

The silicon detector design has been optimized in order to obtain a good position resolution.

The main features of the silicon detector such as implant width and interstrip capacitance have been chosen in order to have more than one strip per cluster while at the same time maintaining the signal high enough on the readout strips to generate a trigger even when the particle crosses the floating ones.

Fig. 9 shows the beam profile measured by the ladder (upper plot) and the correlation between the ladder and one of the x telescope position (lower plot).

The following method has been used to define a cluster in each event:

- The pulse height of each strip PH_i is defined as

  $$\mathrm{PH}_i = \mathrm{raw}_i - \mathrm{ped}_i - \mathrm{CM}$$

  where raw_i is the raw content of the readout channel, ped_i the channel pedestal and CM the common mode contribution for the event;
- the strip with the maximum signal is found; its signal has to be greater than 5 times the noise rms of the strip itself (σ_i);
- the strips contiguous to the one with the maximum signal are considered when they are characterized by a ratio $\mathrm{PH}_i/\sigma_i > 3$. This group of strips is called a cluster.

The choice of the cuts for the strip with the maximum signal (5σ) and for the nearby ones (3σ) is explained by Fig. 10, where the "pull" (defined as the ratio of the strip PH and its noise) for the strip with the maximum signal (upper plot) and for the noise (lower plot) is represented. In the upper plot, the peak on the left is the one due to the noise while the other two correspond to the case in which the particle crosses a readout strip (higher signal) or a floating one (lower signal).

The cluster pulse height (most probable value) as a function of the incidence angle of the beam is shown in Fig. 11. The fit with a $1/\cos\theta$ function is superimposed.

Fig. 12 shows the cluster pulse height in ADC counts (upper plot) and the SNR (lower plot) defined as

$$\mathrm{SNR} = \frac{\sum_i \mathrm{PH}_i}{N_\mathrm{c}} = \frac{\sum_i \mathrm{PH}_i}{\sqrt{\frac{\sum_i \sigma_i^2}{N}}}$$

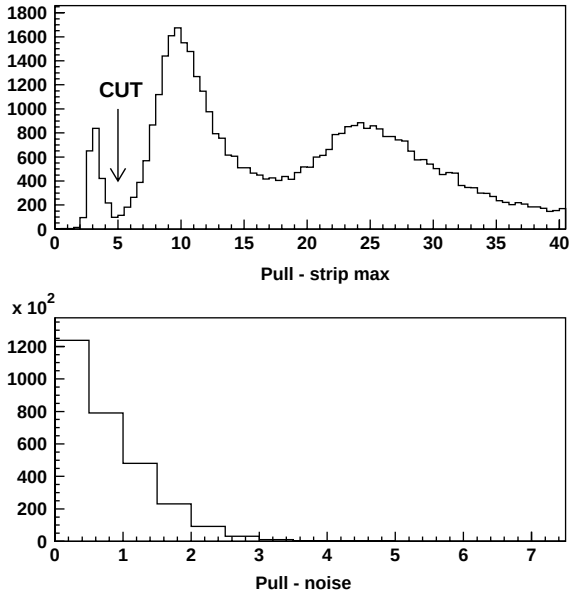

Fig. 10. Upper plot: pull distribution for the strip with the maximum signal. Lower plot: pull distribution for the noise.

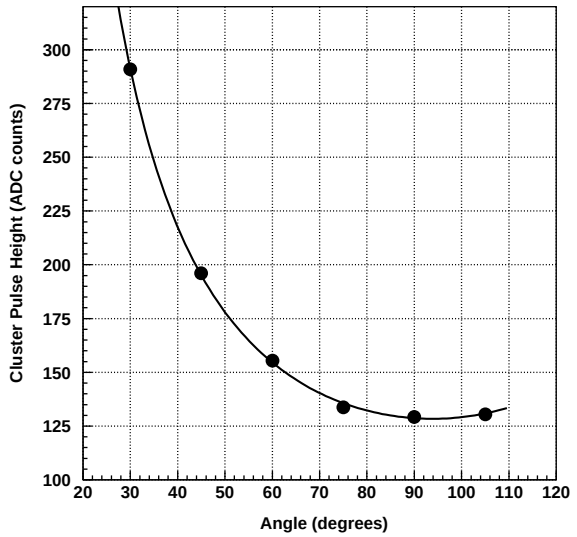

Fig. 11. Cluster pulse height as a function of the incidence angle of the beam with respect to the strip plane. The fit has been performed with a $1/\cos\theta$ function.

where the sum is made over the strips of the cluster, PH_i is the pulse height of the ith strip, N_c is the cluster noise, σ_i is the noise value of the ith strip and N is the total number of strips in the cluster [13].

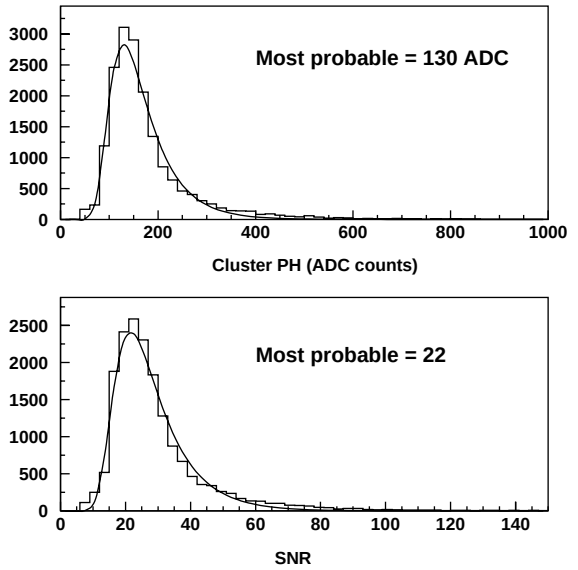

Fig. 12. Cluster pulse height (upper plot) and SNR (lower plot) for an incident beam perpendicular to the detector plane. The fit has been done with a simplified Landau function described in the text.

Both histograms have been obtained with a beam perpendicular to the detector and they have been fitted with a simplified Landau function [14]

$$F(\lambda) = \frac{1}{\sqrt{2\pi}} \exp^{-0.5(\lambda+\exp^{-\lambda})}$$

where ΔE_{MP} is the most probable value of the function, $\lambda = (\Delta E - \Delta E_{MP})/\xi$ and $\xi = \mathrm{FWHM}/4.02$.

The number of strips per cluster as a function of the incidence angle of the beam is shown in Fig. 13. Even for large angles with respect to the pointing direction of AGILE, the mean value is below 5. This means that all the relevant information on the cluster can be transmitted to ground, even with a limited telemetry bandwidth.

3.2.3. Position resolution

To evaluate the position resolution of the AGILE silicon detector, the track was reconstructed using the information of the silicon telescopes nearest to the ladder and the distribution of the residuals, that is the distribution of the difference of the extrapolated position on the

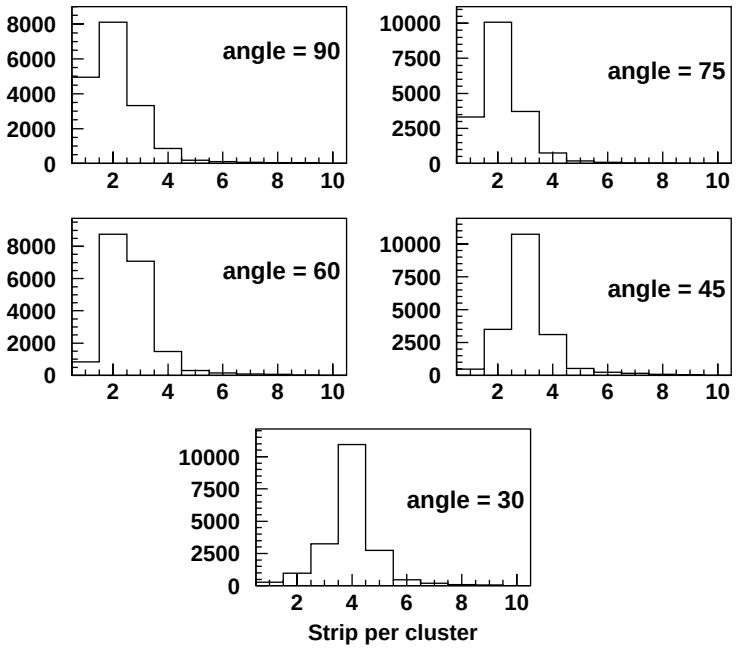

Fig. 13. Number of strips per cluster as a function of the incidence angle of the beam.

ladder and the one measured by the ladder itself, was plotted.

The ladder measured position is computed with a center of gravity method, weighting the position of each cluster strip with the pulse height of the strip itself.

Since the beam momentum is low (2 GeV/c), the multiple scattering due to the material between the two telescopes has to be taken into account. The multiple scattering contribution to the telescope position resolution has been measured replacing the ladder with the third telescope. The result has been compared with the theoretical calculation and the simulation.

The residual distribution obtained with a normal incidence beam of 2 GeV/c is shown in Fig. 14.

The position resolution can be derived from the sigma of the Gaussian fit σ_{fit} as

$$\sigma_{\text{res}} = \sqrt{\sigma_{\text{fit}}^2 - \sigma_{\text{ext}}^2}$$

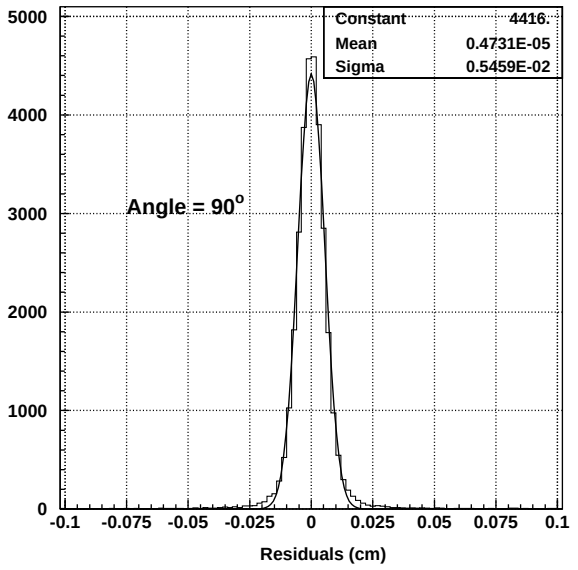

Fig. 14. Position resolution at normal incidence of the beam. The value obtained with the fit is the convolution of the real position resolution of the ladder and of the error introduced by reconstructing the track with the telescopes.

where σ_{ext} is the uncertainty introduced by the track reconstruction of the silicon telescopes, which is due to the multiple scattering.

The position resolution of the AGILE detector as a function of the incidence angle of the beam is presented in Table 3.

Fig. 15 shows the advantage, in terms of spatial resolution, resulting from using the analog information on the charge collected by the silicon strips. As far as the digital evaluation is concerned, the cluster is identified by applying a 3σ cut to the strips and the hit position is the center of gravity of the cluster (in this case, all the strips in the cluster have the same weight).

Table 3
Position resolution of the AGILE detector as a function of the incidence angle of the beam

Angle (°)	σ_{fit} (μm)	σ_{res} (μm)
90	55	47
75	47	37
60	51	41.3
45	67	59
30	116	110

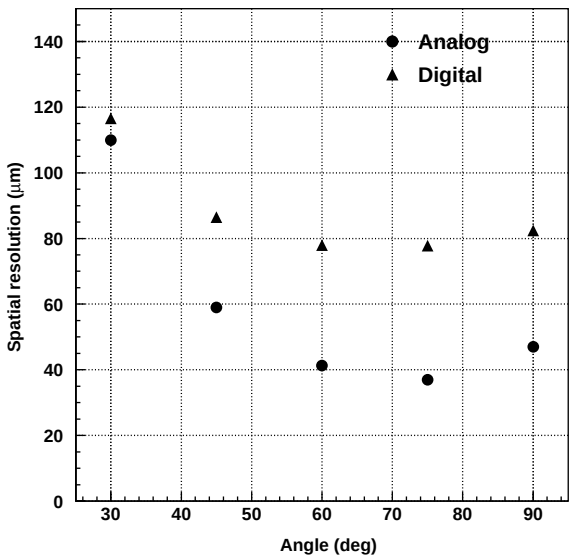

Fig. 15. Comparison between the digital and the analog position resolution for the AGILE silicon detector.

3.2.4. Trigger efficiency

One of the most innovative features of the AGILE Tracker is represented by the autotrigger capability.

Dedicated runs have been performed in order to study the trigger efficiency of the silicon strips as a function of the incident angle of the beam. The efficiency is evaluated considering for each threshold the number of events with a high pulse height in the strip with the maximum and no trigger signal. The presence of a trigger signal is measured with a multihit TDC that follows the time development of the trigger signal itself since it samples up to 16 transitions.

Fig. 16 shows the time interval (y-axis) in μs between the particle crossing and the trigger signal generation as a function of the signal amplitude (x-axis) in the strip with the maximum. The plot has been obtained with a 2 GeV/c beam impinging orthogonally on the silicon detector. The TA1 threshold has been set to 50 keV (0.5MIP).

The lower the pulse height, the higher the time needed to generate the trigger.

From the trigger efficiency point of view, the worst condition is represented by a particle crossing a floating strip, which corresponds to the

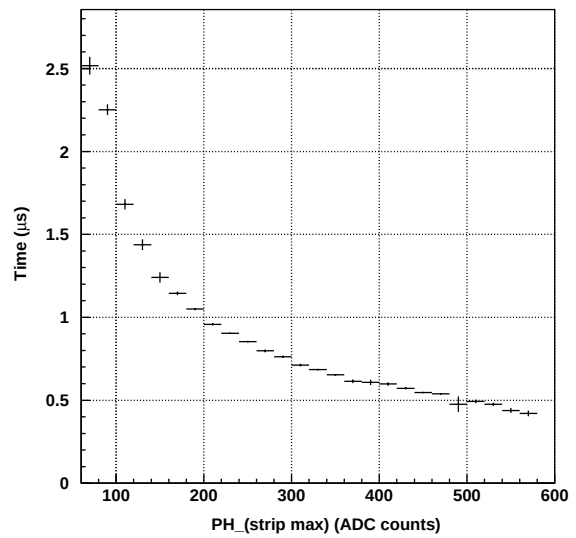

Fig. 16. Time interval between the particle crossing and the trigger signal generation as a function of the signal amplitude in the strip with the maximum.

minimum signal seen by the nearby readout ones. Fig. 17 shows the signal amplitude of the strip with the maximum as a function of the incidence angle of the beam for the two extreme cases of the particle crossing the center of a readout strip or of a floating strip. The line represents a threshold of 1/4 of a MIP. The signal amplitude corresponds to the most probable value of the Landau function (upper plot in Fig. 12).

For all the angles the signal is higher than the threshold, ensuring the maximum trigger efficiency. If the detector noise increases, thus requiring an increase in the threshold value, the efficiency will decrease for tracks impinging orthogonally. Fig. 18 shows the efficiency as a function of the threshold value for two incident angles of the beam. The measured efficiency values are written in Table 4.

3.3. Comparison between data and simulation

From the testbeam data, it is possible to evaluate a set of detector parameters which are fundamental for the simulation of the behaviour of the entire satellite.

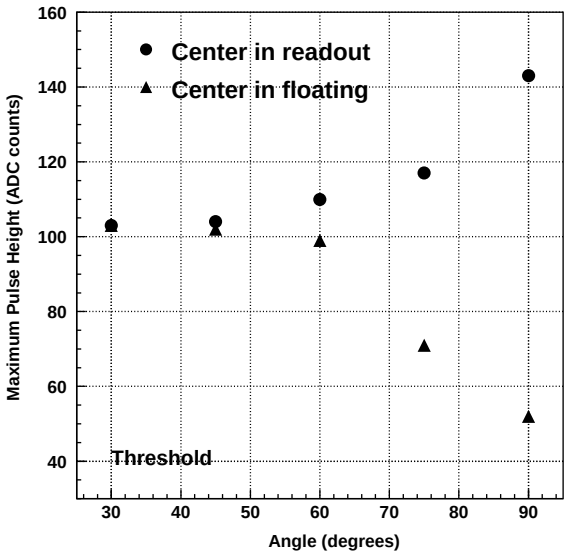

Fig. 17. Signal amplitude of the strip with the maximum as a function of the incidence angle of the beam for the two extreme cases of a particle crossing the center of a readout strip or of a floating one.

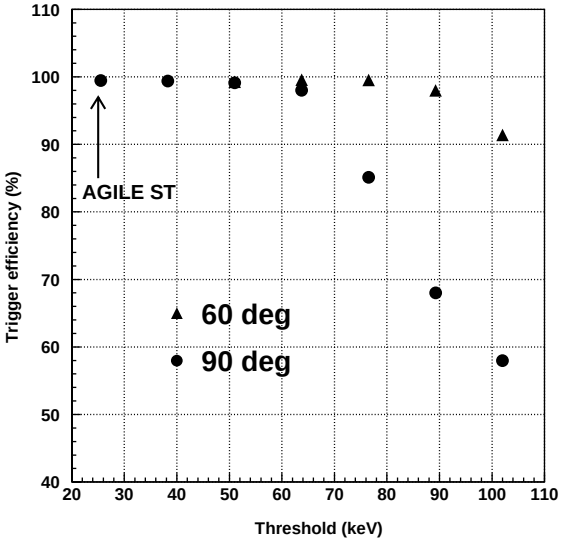

Fig. 18. Trigger efficiency as a function of the threshold value for a 2 GeV/c beam impinging orthogonally and at 60° with respect to the detector plane.

Table 4
Trigger efficiency as a function of the threshold value for an incident angle of the beam of 60° and 90°

Threshold (keV)	ε (%) at 90°	ε (%) at 60°
25	99.46	
38	99.4	
51	99.13	99.25
64	98	99.57
76	85.1	99.55
89	68	98
102	58	91.4

The testbeam setup has been simulated using GEANT 3.21 [15].

The silicon strips are implemented by dividing the silicon itself in slices of 121 μm and the energy information of each of these sub-volumes is saved for each event.

The capacitive coupling between the strips is implemented as described in Fig. 19: the energy released in each strip is multiplied by a factor and assigned to the nearby readout strips. This procedure is applied to each event and to all the strips, and the signal obtained has to be compared with the measured one.

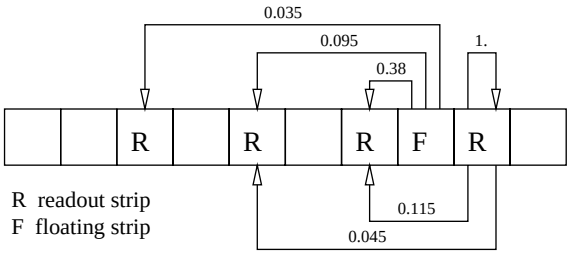

Fig. 19. Schematic representation of the implementation of the capacitive coupling in the simulation. The symmetric couplings on the right are not represented.

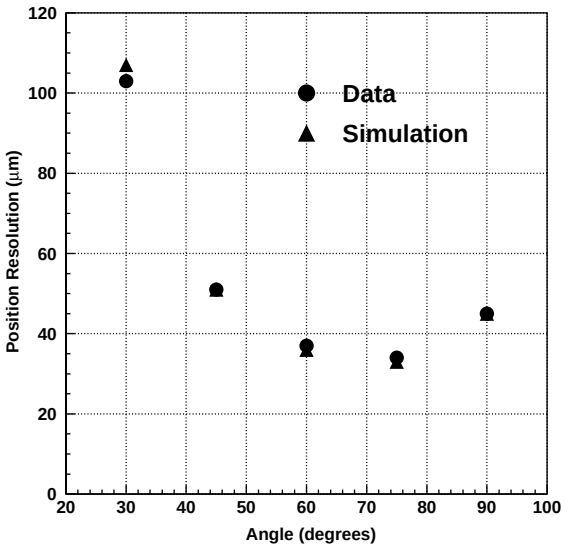

Fig. 20. Comparison of the position resolution as a function of the incidence angle for data and simulation.

The comparison of the position resolution as a function of the incidence angle for data and simulation is shown in Fig. 20.

Fig. 21 shows the comparison data-simulation for the function η which represents the way the signal is divided between adjacent strips

$$\eta = \frac{PH_{max} - PH_{max-1}}{PH_{max} + PH_{max+1}} \quad \text{if } PH_{max-1} > PH_{max+1}$$
$$= \frac{PH_{max+1} - PH_{max}}{PH_{max+1} + PH_{max}} \quad \text{if } PH_{max+1} > PH_{max-1}$$

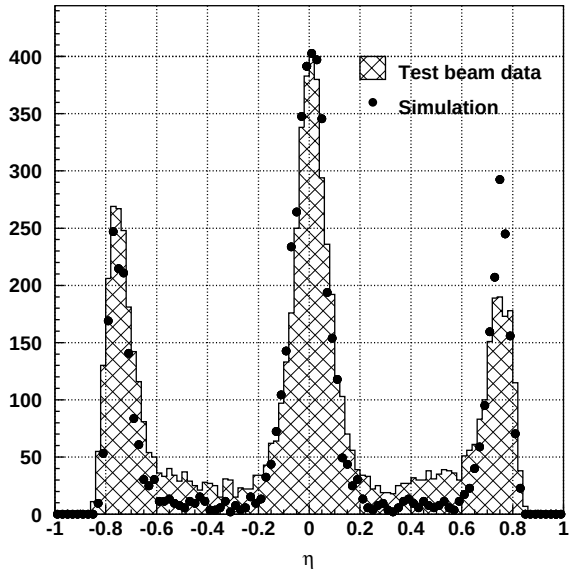

Fig. 21. η function: comparison between data and simulation.

where PH_{max} is the signal of the strip with the maximum and $PH_{max\pm1}$ is the signal of the nearby strip with the higher signal.

4. Conclusions

The Silicon Tracker design has been proved to fully satisfy the scientific requirements set by the AGILE mission.

The testbeam analysis has demonstrated the validity of the analog readout and of the floating strip principle even with a large pitch detector as this one. In this way, it is possible to maintain under control the number of channels and thus the power needed by the instrument while at the same time obtaining a good spatial resolution.

No stability problems have arisen in the use of the ensemble detector-electronics, which is a fundamental aspect for a satellite experiment.

The final production of the AGILE silicon detectors has been completed before the middle of the year 2001.

Around 43 000 silicon channels will be launched in 2003 for a total of 4 m^2 of silicon detectors, which is the largest number of silicon strips as far as satellites are concerned up to now.

Acknowledgements

This work has been done with the financial support of ASI and INFN. We would like to thank Thomas Ruf and the CERN EP and PS division staff for the support during the testbeam and Peter Weilhammer and Alan Rudge for the silicon telescopes.

References

[1] A. Peisert, Silicon microstrip detectors, in: F. Sauli (Ed.), DELPHI 92-143 MVX 2, 1992, chapter of a volume on Instrumentation on High energy Physics, World Scientific Publishing Co., Singapore, 1992;
M. Krammer, H. Pernegger, Nucl. Instr. and Meth. A 397 (1997) 232.
[2] S.p.A. Mipot, Cormons, GO, Italy, http://www.mipot.-com.
[3] IDE AS, Norway, http://www.ideas.no, http://193.216.193.195/download/ASICdocuments/TA1.pdf.
[4] CERN PS East Hall, http://psschedule.web.cern.ch/PSschedule/pindex.html.
[5] G. Vismara, A. Manarin, LEP/BI-TA/Note 85-3, CERN, Geneva, 1985.
[6] A. Rudge, P. Weilhammer, CERN.
[7] O. Toker, et al., Nucl. Instr. and Meth. A 340 (1994) 572.
[8] Sun Microsystems, Inc., DARPA RFC 1050 Remote Procedure Call Protocol Specification (1988).
[9] SBS Bit3 Operations, St. Paul, MN, USA. VME driver provided by Nata Kruszynska (http://www.nikhef.nl/user/natalia/projects/vmehb.html).
[10] J.K. Ousterhout, Tcl and the Tk Toolkit, Addison-Wesley Publishing Company, Reading, MA, 1996.
[11] CN/ASD Group, HIGZ/HPLOT Users Guide, Program Library Q120 and Y251, CERN (1993).
[12] G. Barichello, et al., Nucl. Instr. and Meth. A 413 (1998) 17.
[13] C. Eklund, et al., Nucl. Instr. and Meth. A 430 (1999) 321.
[14] J.E. Moyal, Philos. Mag. 46 (1955) 263.
[15] R. Brun, et al., GEANT detector description and simulation tool, CERN Program Library, 1993.